

SYMBIOTIC STAR CANDIDATES IN GAIA DATA RELEASE 3

SAMANTHA E. BALL¹, BENJAMIN C. BROMLEY¹, AND SCOTT J. KENYON²

¹Department of Physics and Astronomy, University of Utah, 115 S 1400 E, Salt Lake City, UT, 84112, USA and
²Smithsonian Astrophysical Observatory, 60 Garden Street, Cambridge, MA 02138, USA

Version June 26, 2025

ABSTRACT

Symbiotic stars, binary pairs with a cool giant fueling accretion onto a hot compact companion, offer unique insights to our understanding of stellar evolution. Yet, only a few hundred symbiotic stars are confirmed. Here, we report on a new search for symbiotic star candidates in Gaia Data Release 3 (GDR3), based entirely on astrometric, photometric, and spectroscopic information. To begin our search, we identified known symbiotic stars in GDR3 and assessed their absolute magnitude and colors, which are dominated by the cool giant. We also considered measures of astrometric quality that might be affected by binary motion in these systems. Finally, from those sources with Gaia spectroscopic data, we built a low-resolution spectral template that characterizes the unique features of these systems, including H α emission from interaction with the giant’s wind and radiation from the hot star. We then queried the full Gaia DR3 archive for sources with spectroscopic data that are bright (< 17 mag in G-band), have modest relative parallax uncertainties ($< 20\%$), and fall within a region of color–magnitude space characteristic of red giants, keeping only sources with spectra that quantitatively match our template. A machine-learning algorithm, trained on known symbiotic stars, produced a new catalog of 1,674 sources. From cross-matches with infrared and X-ray surveys, we present 25 of these sources as particularly compelling candidates for new symbiotic stars.

Subject headings: Symbiotic stars, Machine learning, Spectroscopy

1. INTRODUCTION

Symbiotic stars are cosmic rarities. They are interacting binaries with a red giant star shedding mass onto a hot companion (Boyarchuk 1969; Bath 1977; Allen 1984; Kenyon & Webbink 1984; Kenyon 1986; Webbink et al. 1987; Munari 2019). The hotter star — a solar-type main sequence star, white dwarf, or neutron star — accretes material from a wind or Roche-lobe overflow from its cooler companion, a red giant, carbon star or Mira variable. When the hot star is a white dwarf, mass transfer generates additional energy from nuclear burning, driving occasional outbursts or steady high-energy emission (e.g., Luna et al. 2013). A more spectacular outcome, a Type Ia supernova, may result if the compact star reaches its Chandrasekhar limit (Kenyon et al. 1993; Hachisu et al. 1999; Liu et al. 2023). Thus, as progenitors of the premier standard candle in cosmology (Riess et al. 1998), symbiotic stars play a critical role in our understanding of the overall evolution of the universe.

The unusual configuration of symbiotic stars, each with a hot and cool binary partner, leads to a unique spectral signature. Thermal emission from the compact hot star contributes to a blue continuum, while the cooler giant dominates the red spectrum. Molecular absorption lines from the giant star’s atmosphere appear alongside emission from ionized species including O III, He II, and hydrogen (H α , H β) (Kenyon & Fernandez-Castro 1987), as

the compact star ionizes material lost by the giant. This combination of a double peaked continuum, absorption features and emission lines from highly ionized atoms distinguishes symbiotic stars from other interacting binary systems — cataclysmic variables (a white dwarf and main-sequence companion) and X-ray binaries (a main sequence star in close orbit with a neutron star or black hole).

Other key observational features of symbiotic stars emerge in photometric imaging and astrometric data. Photometry captures brightness variations that enable precise determinations of stellar magnitudes, temperatures, and variability. In symbiotic stars, the complex interactions between binary partners lead to distinctive light curves, including periodic and eruptive variations (e.g., Merc et al. 2020). Symbiotic binary partners also tend to be widely separated ($\gtrsim 1$ au) compared with other interacting binaries, enabling high-resolution imaging to distinguish components (e.g., Bujarrabal et al. 2020; Planquart et al. 2025). Astrometric data from symbiotic stars contributes to refinements of stellar luminosities as well as their distribution within the Galaxy. These unique characteristics allow symbiotic systems to be distinguished from other binary and single-star systems. These same features — evidence of a cool giant with molecular absorption features coupled with the clear signature of hot gas — guided pioneers in the discovery of symbiotic stars (Merrill & Humason 1932; Swings & Struve 1941; Payne-Gaposchkin 1946).

To date, over 300 symbiotic stars are listed in the SIM-

samantha.e.ball.00@gmail.com
bromley@physics.utah.edu
skenyon@cfa.harvard.edu

BAD astronomical database. This census, while impressive given observational challenges in the identification of individual stars (e.g. Merc & Boffin 2025), is significantly less than theoretical predictions for the population of symbiotic stars in the Milky Way, which range from 10^3 to 10^5 (Kenyon 1986; Munari & Renzini 1992a; Magrini et al. 2003; Lü et al. 2006; Akras 2023; Xu et al. 2024). This discrepancy continues to drive searches for these rare objects, with strategies that focus on optical line emission surveys, along with IR (Akras et al. 2019a, 2021; Chen et al. 2025), UV (Akras 2023), and X-ray (Munari et al. 2021) wave bands. These studies, including others that incorporate machine learning (Akras et al. 2019b; Jia et al. 2023), have yielded dozens of candidates, though far fewer confirmed symbiotic stars.

Here our focus is on the discovery of symbiotic stars, casting a wide, loosely knit net to retrieve high-potential sources for follow-up observations. We use observations from the European Space Agency’s Gaia satellite, which has provided astrometry and photometric data for over a billion stars (Gaia Collaboration et al. 2023, Data Release 3, hereafter GDR3). Low-resolution spectra are available for over 200 million of these sources. Using known symbiotic stars from SIMBAD (Wenger et al. 2000), we train a machine learning (ML) algorithm to identify promising candidates (Akras et al. 2019b; Jia et al. 2023). We describe this approach in §3.1. Then we apply the ML algorithm to a subset of stars in GDR3 to obtain a new catalog of these candidates (§4). We conclude in §5.

2. A CATALOG OF KNOWN SYMBIOTIC STARS

Symbiotic stars have emerged as a distinct class of stars because of their spectral features. Indeed, these objects began to stand out roughly a century ago as a result of discoveries by Cannon, Merrill and Payne-Gaposhkin (see Kenyon 1986, for a historical summary). While Gaia is foremost an astrometric database, it provides photometry, even in the time domain (cf. Merc et al. 2020). It also contains spectroscopic information in the form of spectral template coefficients for about 10% of the DR3 sources. Our approach here is to gather this information for known symbiotic stars and to train a machine learning algorithm to identify promising symbiotic star candidates. We begin with our collection of known symbiotic stars.

2.1. Symbiotic stars in Gaia with low-resolution spectra

To identify known symbiotic stars, we queried the SIMBAD database (Wenger et al. 2000) seeking sources with object types Sy* and skipping stars listed as object type Sy?. The result yields 302 known symbiotic stars. SIMBAD provided a GDR3 `source_id` for 243 of these objects. We reviewed the leftover 59 stars with Aladin Lite (Bonnarel et al. 2000) using the coordinates given in SIMBAD to manually match GDR3 sources. Of the 59 stars, five have both a manually matched GDR3 `source_id` and Gaia spectral data (true-valued `has_xp_continuous` flag). One star, with SIMBAD `main_id` EM* AS 269, was excluded because there were two GDR3 close sources with comparable magnitudes, making it difficult to distinguish the symbiotic star. This procedure defines our catalog, 248 sources that are recognized in SIMBAD as symbiotic stars and

TABLE 1
SYMBIOTIC STARS MANUALLY MATCHED WITH SPECTRA DATA

SIMBAD	ra (ICRS)	dec (ICRS)	Gaia <code>source_id</code>
V* V916 Sco	17 43 54.7	−36 03 26.5	4040972692694908928
PN K 3-22	19 09 26.6	+12 00 44.6	4313125288215049728
V* V4073 Sgr	18 08 19.1	−22 57 19.0	4066601273532526336
PN Th 3-29	17 32 27.9	−29 05 08.8	4058843158219588480
VVV NV003	17 50 19.3	−33 39 07.3	4041878930741533824

that have GDR3 spectra. Table 1 below lists the five objects we matched to GDR3, while the online version has all 248 stars. Of these sources, 224 are listed as confirmed symbiotic stars in Table 6 of Akras et al. (2019a).

2.2. Photometric properties

We illustrate attributes of the 248 stars selected here, starting with a Hertzsprung-Russel (HR) diagram in Figure 1. The HR diagram emphasizes that symbiotic stars are post-main-sequence giants, with sources broadly clustered around a `bp_rp` color index of ~ 2 and an absolute magnitude of around -2 in Gaia’s G band. There are a few exceptions, with a handful of sources that appear near the main sequence, and two that are unphysically bright. These outliers tend to have poorly constrained distances (low `parallax_over_error`) or high levels of extinction (e.g., high `ag_gspphot`). The figure also indicates cross-matches in all-sky X-ray surveys from *ROSAT* (Aschenbach et al. 1981; White et al. 2000), *XMM-Newton* (Jansen et al. 2001; Webb et al. 2020), and *SRG/eROSITA* (Predehl et al. 2006; Freund et al. 2024), with a total of 59 sources identified in at least one of these catalogs (Table 1, online version). Almost a quarter of our selected stars are plausible X-ray emitters, which is a much larger fraction than in the general population of red giants (e.g., Hunsch et al. 1998; Schmitt et al. 2024) as a result of interactions between the symbiotic stars’ binaries and the mass flowing between them.

Figure 1 shows a “selection zone” in the color-magnitude plane that we use below to seek symbiotic star candidates (§3.1). It is defined with these criteria:

$$1.0 < \text{bp_rp} < 7 \text{ mag} \quad (1)$$

$$-6 \text{ mag} < M_G < \min(1.8 \times \text{bp_rp} - 3.4) \text{ mag},$$

where M_G refers to the absolute magnitude in Gaia G band. Within this region lie typical red giants. In our collection of 248 sources, 221 have GDR3 low-resolution spectra, and of these stars, 171 reside on our selected part of the HR diagram. This group of sources constitutes our symbiotic star catalog.

In addition to red giants, our catalog contains some noteworthy sources near the perimeter of our selection zone. For example, close to the bright edge is WY Vel, flagged as a variable by Cannon (see Shapley 1923). It is a red supergiant with a B-star companion (Buss & Snow 1988; Healy et al. 2024), designated as a VV Cep-type star in the online database of symbiotic stars maintained by Merc et al. (2019). Similarly, 17 Lep, just interior to the blue edge of our selected region, is a spectroscopic binary with a red giant and an A-star; mass transfer onto an accretion disk appears to be the result of wind from the red giant (Blind et al. 2011). We include these sources to leave open the possibility of identifying new

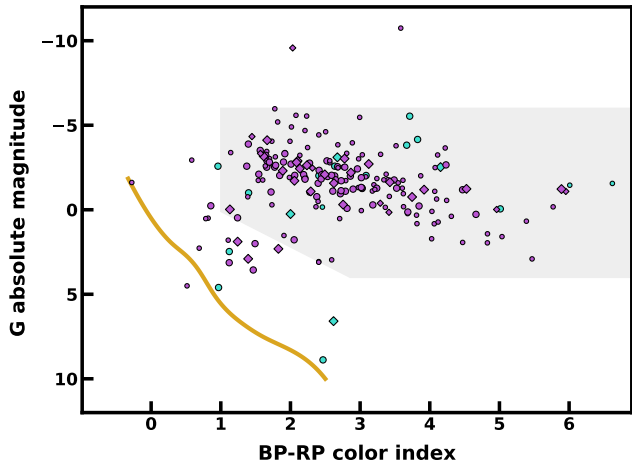


FIG. 1.— A Hertzsprung-Russel diagram for the 248 symbiotic stars highlighted in this study. Each point is derived from GRD3 parameters. Most of the sources (224, violet markers) are confirmed in Akras et al. (2019a, Table 6 therein), while the remaining 24 were identified here with SIMBAD (blue-green markers). The larger points indicate that the GDR3’s parallax error is less than 20%. The shape of the symbol indicates whether a star is associated with an X-ray source (diamond) or not (circle). The smaller points thus correspond to sources that have less certain distance moduli. For reference, a cartoon curve (lower left) illustrates the approximate location of the main-sequence ridge in the Gaia survey.

candidates, cognizant that location within the selection zone may be important to the ultimate identification of symbiotic stars.

One feature of the HR diagram in Figure 1 is that sources are not corrected for extinction or reddening. For many stars in our catalog, Gaia provides estimates (`ag_gspphot` and `ebpminrp_gspphot`), while most others appear in the Bayestar (Green et al. 2019) and DeCAPS (Zucker et al. 2025) 3D dust maps, from which we glean that extinction and reddening can be significant. Figure 2 shows some evidence in a G-J and J-K color-color diagram for Gaia G band, with J and K bands from SIMBAD. There is a discernible correlation between these color indices and the reported extinction in GDR3, indicating mid-infrared absorption and dust, either interstellar or intrinsic to the stellar systems. The figure also shows colors derived from the Wide-field Infrared Survey Explorer (WISE; Wright et al. 2010; Cutri et al. 2013), W1-W3 and W2-W4, to probe intrinsic dust emission. A connection with `ag_gspphot` is less clear. These mixed results suggest that the extinction and reddening are the result of dust in an indistinguishable mix of interstellar grains along the line of sight (as estimated by 3D dust maps) and dust produced by red giant winds, leading to enrichment of the local environment.

When interstellar extinction is small, color-color relations distinguish distinct types of symbiotic stars (Webster & Allen 1975). S-type stars have comparatively sparse amounts of dust in the surrounding environment. Their optical and near-infrared (NIR) colors reflect the cool giant’s atmosphere with typical effective temperatures of a few thousand Kelvin. D-type symbiotic stars harbor a Mira variable, a late-stage red giant that produces enough dust to impact NIR flux through absorbed and reprocessed starlight. The temperature of the dust in D-type stars is typically below a thousand Kelvin. A

third class, D-type/ stars, is thought to have a younger, yellow giant (e.g. Akras et al. 2019a, and references therein).

Figure 2 illustrates that the population of 171 symbiotic stars considered here have a range of colors in optical and NIR with a clustering in J-K between 1 to 2 mag, typical of red giants. Approximately a quarter of the stars show a NIR excess, with J-K above 2 mag. Interpreting the excess as a sign of the presence of dust, we note that the fraction with J-K > 2 (26%) is comparable to the fraction of D-type stars in the total symbiotic star population (~20% Belczyński et al. 2000; Akras et al. 2019a). WISE W1-W3 and W2-W4 colors yield a similar picture. The majority of sources are clustered near W1-W3 \approx 0.5 and W2-W4 \approx 1, presumably representing S-type stars. About 13% of the sources are redder than 2 mag in J-K, with W1-W3 > 1 and W2-W4 > 2, as expected for D-type stars.

Despite the prominent role of dust in symbiotic stars and the possibility of interstellar reddening and extinction, here we do not attempt corrections to color and magnitude. Instead, we select for a broader range in color-magnitude space (Eq. (1)) to admit candidates that may be reddened or extinguished, whatever the reason.

2.3. Astrometric considerations

The identification of symbiotic stars is facilitated by accurate astrometry, a requirement for precise absolute magnitude calculations. Yet symbiotic stars present a potential challenge. As binaries with the center of visible light tied to the orbiting bright giant, these objects have orbital motion that impacts astrometric measurement. The effect is most acute when the orbital period is comparable to the time baseline of the astrometric observations. Symbiotic stars consist of roughly solar-mass partners with separations of a few astronomical units, and their orbital periods are that of a couple of years, remarkably similar to the 34-month baseline of GDR3 (Gaia Collaboration et al. 2023). Binaries with closer separations and more rapid binary motion would not be resolved by Gaia, while more widely separated pairs have slower orbital motion that does not affect the mutual linear drift that Gaia measures.

To assess the impact of binarity on Gaia astrometry, we consider the relative change of sky position as a result of orbital motion (Stassun & Torres 2021). For a binary star with separation of 2 au, this motion may shift the sky position of a companion by

$$\Delta p \approx 2 \times \left[\frac{p_0}{1 \text{ mas}} \right] \text{ mas}, \quad (2)$$

where p_0 is the parallax in the absence of orbital motion. This shift is roughly equivalent to p_0 , and is in principle, measurable so long as parallax errors are comparatively low. Adopting a value of $O(0.1)$ mas for the astrometric errors generally, we expect that orbital motion binary stars with $p_0 \gtrsim 0.1$ mas may negatively impact astrometric fits to linear drift, if the orbital period is comparable to GDR3’s \sim 3 year time baseline (for example, Penderghast *et al.*, in preparation). The measure of quality of astrometric fitting in GDR3, `ruwe`, is a key indicator of potential binarity; low values indicated good fits, while values above 1.3 are poor, and have been specifically associated with orbital motion (Stassun & Torres

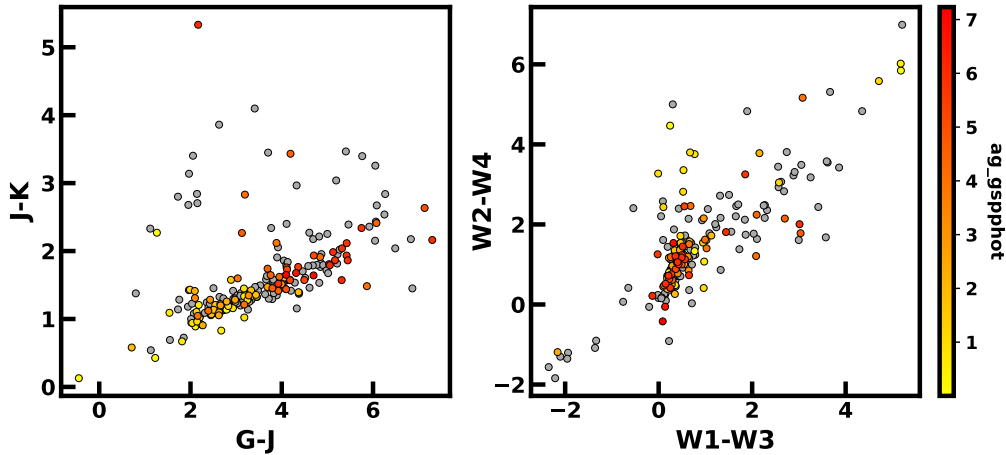


FIG. 2.— Color-color diagrams of known symbiotic stars in our catalog of 248 sources. In the left plot, J and K magnitudes are from SIMBAD, while the G-band magnitudes are from the `phot_g_mean_mag` column in the GDR3 main source catalog. On the right are WISE colors. The symbol color of each point designates the extinction (`ag_gspphot`), provided in the Gaia archive, unless it is not provided (gray points).

2021; Kervella et al. 2022; Pearce et al. 2022; Whiting et al. 2023; Castro-Ginard et al. 2024).

Figure 3, provides some evidence of this effect in our catalog of symbiotic stars. The majority of the dozen stars with parallax above 1 mas, where orbital motion is clearly resolvable, have `ruwe` well above 1.3, as expected. Stars with parallax below about 0.1 mas have predominantly low `ruwe`, since orbital motion is lost in the noise. In between, stars show a mix of high and low `ruwe`, though the majority trend to lower values. We conclude that `ruwe` is a potentially useful indicator of symbiotic stars, though not a strong one.

Figure 3 distinguishes sources two ways. First, the figure shows X-ray cross-matches (diamond-shape symbols) for comparison with sources with no detected X-ray emission. The X-ray bright sources are concentrated at distances within a few kiloparsecs, the result of flux limits in the survey (e.g., Freund et al. 2024). Second, Figure 3 distinguishes sources that have accurate parallaxes (`parallax_over_error` > 5) from those that do not. As expected, more distant sources tend to have lower signal-to-noise in parallax. In light of symbiotic binarity, we might expect to see some close-by objects have high `ruwe` but also low `parallax_over_error`, since parallax error folds into the general astrometry errors that `ruwe` characterizes. Indeed some of this trend is apparent but for sources within about 10 kpc, `ruwe` can still be above 1.3 even when `parallax_over_error` is above 5. This observation gives some hope that `ruwe` may be a valuable indicator for symbiotic stars even when their heliocentric distances are well-measured.

2.4. Gaia low-resolution spectra and projection coefficients

Finally, we come to the low-resolution spectra in BP and RP bands provided in GDR3. We select for true values of `has_xp_continuous` to facilitate comparison spectra from source to source (data are represented with a common set of template functions and easily yield fluxes at a specified set of spectral wavelengths). We adopt 330 logarithmically-spaced sample points spanning

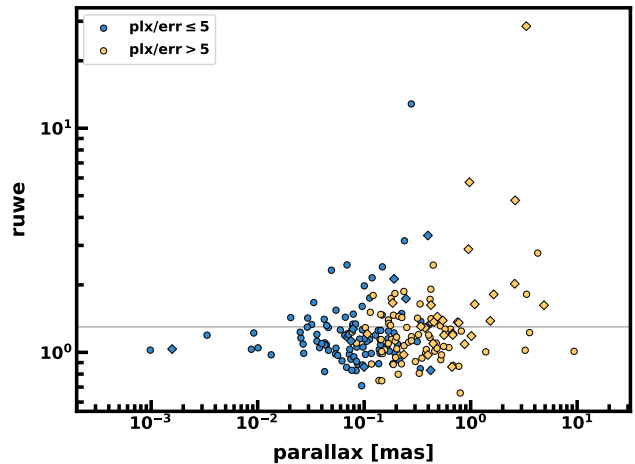


FIG. 3.— The GDR3 astrometric error parameter `ruwe` as a function of parallax. The data is consistent with binary stars at a separation of a couple of astronomical units. Nearby sources have higher overall astrometric errors than distant stars, since the orbital displacement on the plane of the sky is greater. If the orbital separation were much smaller or much larger than a few astronomical units, then orbital motion would not have as much of an impact on Gaia astrometry, with its 34 month baseline. In the former case, orbital periods would be very short and angular displacement of the binary stars would be small. In the latter case, orbital separations would be large, and binary motion would be too small to be measured astrometrically. As in Figure 1, X-ray cross-matches are indicated with a diamond symbol, while others are shown as circles. The distribution of X-ray objects is concentrated toward low distances.

both wavebands over a wavelength range of 361 nm to 1050 nm. We realize each spectrum on this wavelength grid, integrate with Simpson’s rule to find the total flux, then normalize so that the total flux is unity in the units set by the Gaia BP_RP spectrum module `gaiaxy`. We next subtract off a continuum, identified with a Savitsky-Golay smoothing filter (83-point window width and cubic fitting). To highlight distinctive spectral features as opposed to their strength, we then scale these high-pass filtered signals so that their *pointwise* standard deviation is unity.

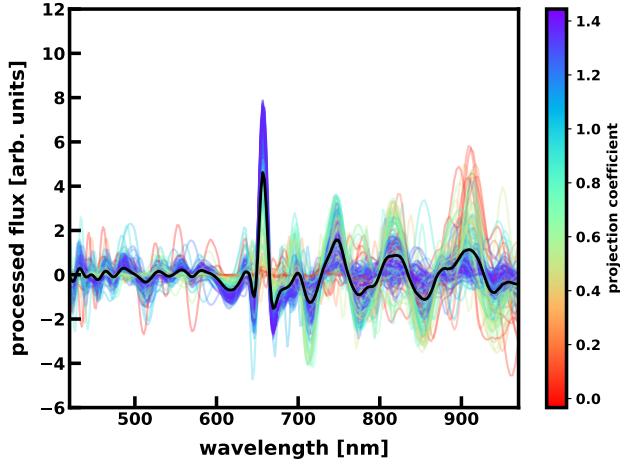


FIG. 4.— GaiaBP_RP spectra of sources in our symbiotic star catalog. The thick black curve is the mean spectrum for the catalog, while the thin curves are individual spectra. Their color indicates a projection coefficient, defined in Equation (3).

Figure 4 shows the spectra constructed in this way for all 171 objects in our catalog. It indicates that a solid group of sources have comparatively strong H α emission and modest TiO absorption bands. The presence of O VI Raman lines near 700 nm, the result of irradiation of cool gas by UV light around symbiotic stars (e.g., Kenyon 1986), may also be perceptible in the spectra. Others have weaker line emission and stronger molecular absorption. Despite these variations, the mean spectrum is a fair representation of individual spectra.

Toward being able to use spectral data to identify symbiotic stars, we quantify the degree to which an individual spectrum matches the mean with a projection coefficient,

$$S_i \equiv \beta(f_i, \bar{f}) = \sum_j f_{ij} \bar{f}_j, \quad (3)$$

where f_{ij} is the flux from the i^{th} star sampled at the j^{th} wavelength in the logarithmically spaced set of points, here chosen to run from 600 nm to 775 nm to focus in on H α and some of the TiO bands, giving both roughly equal weighting. The angular braces denote the catalog average. All spectra are normalized so that $S(f_i, f_i) = S(\bar{f}, \bar{f}) = 1$. The values of S range from about -0.03 to 1.44, with an average of unity (by construction) and a median value of 1.18, and a clustering around $S \approx 1.3$. We illustrate this distribution next.

2.5. Drawing sources from GDR3

For a preliminary assessment of the projection coefficient S as an indicator of symbiotic stars, we perform a random draw from the GDR3 archive from the first ten million sources as ranked by the parameter `random_index`. This draw netted 47,693 sources, hereafter “47k stars,” all lying within our selection zone (Eq. 1), brighter than 17 mag in Gaia G band, with `parallax_over_error` ≥ 5 , and with BP_RP spectral data (the `has_xp_continuous` flag is true). Figure 5 shows a histogram of the projection coefficients of the 47k stars, which are expected to include no more than a few symbiotic stars. The distinction between these sources and symbiotic stars is clear. The vast majority

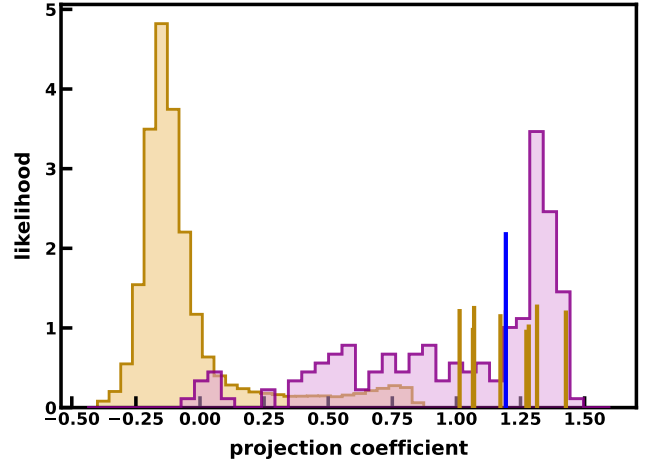


FIG. 5.— Distribution of projection coefficient S from a random draw of over 47,000 sources from Gaia (yellow-tinted histogram) and from our sample of symbiotic stars (violet-tinted histogram). Sources with $S \gtrsim 0$ corresponds to potential symbiotic star candidates in the random draw, but values above $S = 1$ have spectra that more strongly couple to the template function based on the average spectra of known symbiotic stars. The nine sources in the random draw with $S > 1$ are indicated with thin, golden-brown vertical lines, including a taller one, in blue, that corresponds to a known symbiotic star that happened to be in the random draw.

(97%) of the random stars have S values below 0.5, and all but nine lie below $S = 1$. Only five of the random stars lie above the median value of $S = 1.18$ for symbiotic stars. We conclude that S is a robust metric for discriminating symbiotic stars from non-symbiotic stars, and for identifying new symbiotic star candidates.

This example, based on a query of ten million GDR3 sources, represents about 0.6% of the GDR3 archive. Of the nine stars in this group with $S > 1$, one, EM* AS 281, is a known symbiotic source. The other eight sources include promising candidates. For example, EM* AS 276 is a long-period variable centered near the middle of the red giant cluster in our selection zone (Fig. 1). At this rate, we anticipate identifying $\sim 1,500$ new symbiotic star candidates in a search of the full archive.

A higher projection coefficient threshold would yield greater selectivity. For example, adopting $S \geq 1.18$ (the median value for symbiotics) would lead to under a thousand candidates. Alternatively, we can use a machine learning algorithm to perform a more nuanced search that includes specific color, magnitude, and astrometric information. We describe our ultimate approach, a combination of both, next.

3. SEEKING SYMBIOTIC STARS IN GAIA DR3

With the preliminary exploration based on known symbiotic stars and the sample of 47k stars chosen at random to be in our selected color-magnitude zone (Fig. 1) and drawn to be fairly bright (< 17 G mag) and close (by virtue of well-measured parallax, with `parallax_over_error` > 5), we train a machine-learning algorithm to identify symbiotic star candidates. The projection coefficients (§2.4) will play a significant role, but we will also design the algorithm to take advantage of other information, including astrometry, photometry, and color. We introduce our classifier first, and then proceed to our mining operation to net new symbiotic stars in GDR3.

3.1. A machine-learning classifier

To ensure a thorough and well-rounded classifier, we follow this prescription for deriving a machine-learning classifier:

1. Set-up training parameters using a select set of columns from the GDR3 main source table to highlight distance, photometry, color, and astrometric solution. Details are below.
2. Download the Gaia low-resolution spectra and create projection coefficients for each train/test set.
3. Create labels to represent if a star is symbiotic or not.
4. Create classifier parameters to fit the datasets and make a matrix regarding the accuracy of the predicted versus misclassified stars.
5. Gather a list of stars from Gaia from our selected region outlined in §2.
6. Run the classifier, assigning probabilities of a match to symbiotic star properties, and filter the candidates.

In creating the training set, we use the 171 known symbiotic stars within our selected region. In using this list for the machine learning algorithm (hereafter: ML), we want the algorithm to place extra importance on these specific stars. To make sure this happens, we copied the full 171 over into a new dataset at least once, from there we randomly selected from the 171, allowing duplicates, to add up to a list of 1500 total stars. Each source is assigned a label $\ell = 1$. We then obtained a sample of non-symbiotic stars from the 47k stars, randomly selecting 1500 stars for our test dataset. The test dataset was then run through SIMBAD to confirm that it contained no known symbiotic stars. These sources were assigned a label $\ell = 0$. The combined test/train sets totals to 3000 sources. This list was then randomly mixed and split in half (1500 sources) to be tested by the classifier.

In compiling the spectra data, we calculated the projection coefficients (§2.4) of each source and added the column to our test/train datasets for the ML to use (*proj_coeff*, also *S*). We set up additional Gaia attributes on which to further train the data sets. Specifically, we use *bp_rp*, *phot_g_mean_mag*, *parallax*, *parallax_over_error*, *astrometric_gof_al*, *ra*, *dec*, *pmra*, *pmdec*, *ruwe*, and M_G in creating our classifier. The significance of each parameter’s inclusion into our model is outlined as follows.

- *bp_rp* (Blue - Red Color Index): This parameter represents the difference between the BP (blue photometry) and RP (red photometry) magnitudes in the Gaia survey. It serves as a proxy for the intrinsic color of a star, which correlates with stellar temperature and spectral type. The color index is critical for distinguishing between stellar populations and classifying stars by their evolutionary stage. Our prior assumptions on *bp_rp* are built into selection zone (Eq. 1) in the color-magnitude plane.

- *phot_g_mean_mag* (Mean Gaia G-band Magnitude): The mean brightness of an object in Gaia’s broad G-band filter, this parameter is fundamental for assessing the apparent luminosity of a source. When combined with parallax, it enables the derivation of absolute magnitudes, which are crucial for distinguishing between different types of celestial objects, such as main-sequence stars, giants, and white dwarfs.
- *parallax*: This parameter provides direct distance measurements to celestial objects.
- *parallax_over_error*: The signal-to-noise ratio of the parallax measurement, this parameter quantifies the reliability of the distance estimation.
- *astrometric_gof_al* (Astrometric Goodness-of-Fit Along-Scan): This parameter measures the goodness-of-fit of the astrometric solution in the along-scan direction. It is used to assess the quality of Gaia’s astrometric measurements, with larger values potentially indicating binarity, extended sources, or systematic errors.
- *ra* (Right Ascension): This parameter is the measure of an object’s position within the sky, specifically measured east-west in hours along the celestial equator.
- *dec* (Declination): This parameter is the measure of an object’s position within the sky, specifically measured north-south in degrees from the celestial equator.
- *ruwe* (Renormalized Unit Weight Error): This parameter is an indicator of the quality of the astrometric solution. A value significantly greater than unity may indicate binarity when orbital periods are comparable to the Gaia time baseline (e.g., Castro-Ginard et al. 2024; also Penderghast et al., in preparation). The 34-month observations of GDR3 are fortuitously comparable to the expected orbital period of symbiotic stars, so that *ruwe* may be a useful indicator in our search (Fig. 3).
- *pmra* (Proper motion-Right Ascension): This parameter measures the proper motion of an object in the right ascension direction. Proper motion data aides in distinguishing between different stellar populations, such as nearby stars with high proper motion versus distant extragalactic objects with negligible proper motion. This quantity is used to derive the total proper motion, which we adopt as a feature in the machine-learning algorithm.
- *pmdec* (Proper motion-Declination): This parameter measures the proper motion of an object in the declination direction. Like *pmra*, it is used in calculating the total proper motion.
- M_G (absolute magnitude): The intrinsic brightness of sources derived from *phot_g_mean_mag* and *parallax* is a key parameter in the identification of stellar types. This feature-engineering addition

is included in part because of its direct role in the definition of the selection zone along with `bp_rp` in Eq. 1.

- *S* (spectral projection coefficient): Since symbiotic stars are ultimately distinguished by the presence of emission lines from hot gas and absorption bands from cool dust, spectroscopy is essential in a search for them. The Gaia archive provides spectral information in the form of separate *BP* and *RP* coefficients associated with template functions of wavelength. Early investigations used a large subset of these coefficients (>40 parameters) in machine learning, but we performed an extreme dimensional reduction by replacing them with the single projection coefficient in Equation (3). This quantity encodes the main spectral features that make symbiotic stars unique.

We used a parameter grid to fine-tune the Random Forest Classifier for better accuracy. The classifier was then run on the test and training datasets and produced a matrix by which it correctly predicts and/or misclassifies the stars. Figure 6 shows the confusion matrix of our classifier, which displays the classification performance of the ML model used on the test dataset to identify symbiotic stars. Overall, the matrix reflects perfect recall (no missed symbiotics) and high precision, with a 1.0 accuracy. It identified only three false positives out of 1,500 predictions—demonstrating the classifier’s excellent performance in distinguishing symbiotic stars from the non-symbiotic background population.

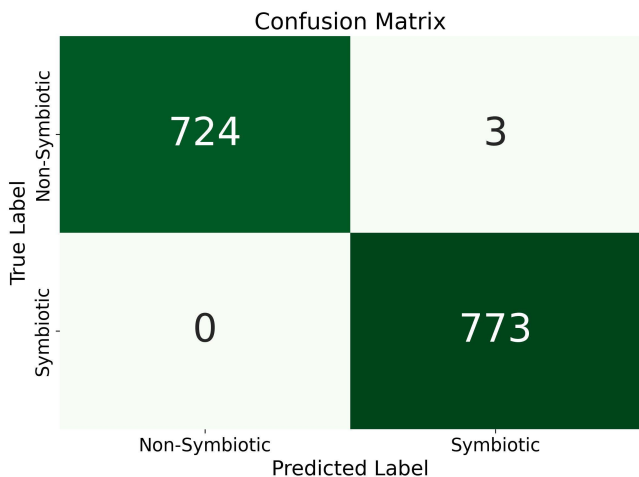


FIG. 6.— Confusion matrix of our classifier. The y-axis represents the true labels, with the top row corresponding to true non-symbiotic stars and the bottom row corresponding to true symbiotic stars. The x-axis represents the predicted labels, where the left column indicates what the model predicted as a non-symbiotic star, and the right column indicates what was predicted as a symbiotic star. The upper-left cell (724) represents true negatives, where the model correctly identified the non-symbiotic stars. The upper-right cell (3) represents false positives, where non-symbiotic stars were incorrectly classified as symbiotics. The bottom-left cell (0) represents false negatives, indicating that the model did not miss any true symbiotic stars. The bottom-right cell (773) represents true positives, where all symbiotic stars were correctly identified by the model.

3.2. Mining GDR3 for symbiotic stars

With a robust machine-learning classifier in place, we select sources from the full GDR3 archive. To come up with a list of candidate symbiotic stars that is manageable, we draw from the archive using the same selection as our 47k stars (eq. 1, `phot_g_mean_mag` < 17, `parallax_over_error` > 5), and further limit our operation to sources with $S > 1$, thus focusing on the peak of the projection coefficient distribution for known symbiotic stars. As roughly anticipated from the 47k stars, this selection nets us 1,790 candidates, including 48 known symbiotic stars among the brighter and closer objects in our catalog.

The next step is to run these sources through the machine-learning classifier.

4. RESULTS: A NEW CATALOG OF SYMBIOTIC STAR CANDIDATES

Here we present the outcome of applying our classifier (§3.1) to the candidate list of stars mined from GDR3 (§3.2). The 1,790 candidates, without removing the known symbiotics therein, were run through the ML. Keeping the known symbiotics into our candidate list was a good indicator to see if the classifier would pick out the already known symbiotics. There were 48 known symbiotics in this selection list, the classifier identified the first 30 stars as true symbiotics while the other 18 stars were still within the top 50 respectively. This test demonstrated the accuracy of the classifier.

After removing the known symbiotics, the ML classifier identified 1,674 stars as candidates with a formal probability $P > 50\%$ of being a symbiotic star. This list includes 182 candidates with a probability P greater than 90%, and 36 stars have $P \geq 95\%$. Table 2 below shows the 15 stars identified by the classifier with the highest formal probability of a symbiotic star classification. The complete Table 2 with all 1,674 candidates is available in this [arXiv](#) submission as an ancillary file in machine-readable format (`table_2.all.csv`), along with a separate README file (`table_2.all_readme.txt`). In both versions, we indicate whether a source has a cross-match in one of the X-ray catalogs considered here (*ROSAT*, *SRG/eROSITA*, and *XMM-Newton*) to highlight candidates that may have active accretion onto a compact symbiotic partner.

To illustrate properties of stars in our catalog of candidates, we first plot a HR diagram in Figure 7. The distribution of sources in the color-magnitude plane generally increases toward the fainter and bluer region of our selection zone in the HR diagram. These objects lie well off the main sequence, but still follow the overall pattern of Gaia sources in this part of the HR diagram, with the number density increasing closer to the main-sequence ridge line. The qualitative impression is that the bulk of our candidates are at least partly reflective of the underlying Gaia source distribution.

Figure 7 also shows known symbiotic stars, which more broadly span the selection zone and are loosely clustered around `bp_rp` ~ 2 and $M_G \sim -2$, typical of red giants. To highlight these clustered stars, we use a threshold

$$M_G < 2.1 * bp_rp - 5, \quad (4)$$

indicated with a gray line in the figure. Of the known symbiotic stars, over 90% are in this red giant region of

TABLE 2
TOP 15 SYMBIOTIC STAR CANDIDATES (ML)

Gaia DR3 Source.ID	RA (degrees)	Dec (degrees)	BP-RP	M_G	Ruwe	S	p	X?
6908433150198135936	309.8358530	-5.2878887	1.875	-2.996	1.345	1.21	0.99	
5328425487860113792	132.9879199	-48.6426061	1.482	-1.211	3.033	1.09	0.98	
5331436642194644992	132.4851801	-45.4742559	1.807	-0.130	3.442	1.11	0.97	
5258349561694308096	151.1261185	-58.6644456	1.389	-2.296	9.827	1.23	0.97	
3034134257044832000	113.3396104	-11.8110711	1.267	0.235	3.792	1.17	0.97	
5862963206161616640	191.9614122	-62.9959058	1.113	-2.863	1.903	1.11	0.97	*
5326692730551766016	136.8472801	-48.8349290	1.978	1.771	3.269	1.20	0.96	
5338064773206447744	165.4309219	-60.5850538	1.266	-1.330	2.803	1.21	0.96	
5350817871109520128	160.0553395	-57.8165306	1.504	-0.123	2.702	1.11	0.96	
5983723702088571392	242.4964422	-48.5744313	1.641	-2.797	1.374	1.13	0.96	
6054125191134238336	183.0719245	-63.8280692	1.402	-0.894	1.945	1.21	0.96	
4067633238255477248	268.3685113	-24.7743574	1.088	-2.883	3.636	1.28	0.96	*
4155000844481174656	278.3656995	-10.5901248	1.988	1.879	8.233	1.17	0.96	*
5528044641382352640	126.6564813	-39.7441306	1.564	0.962	5.276	1.07	0.96	
512813086494390272	21.8378034	64.2855732	1.514	-0.377	2.896	1.24	0.96	

NOTE. — Column M_G refers to Gaia G absolute magnitude, column S is the projection coefficient in Eq. (3), column p is the classifier probability, and in the column labeled X?, an asterisk (*) indicates that a source is associated with X-ray emission.

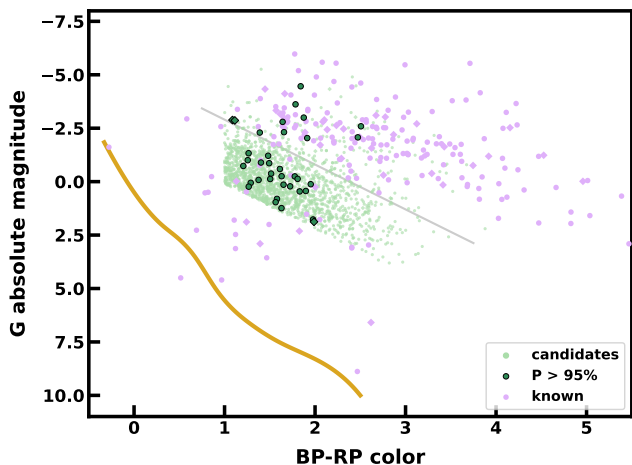


FIG. 7.— A Gaia-based color-magnitude diagram for candidate symbiotic stars, similar to Figure 1. Here, the green-toned symbols show our 1,674 candidates, with those have a formal probability of being a symbiotic star at 95% or greater appear in the darker shade. The faint violet-toned symbols are the known symbiotic stars. As in the earlier figure, the orange curve represents the main sequence. A gray line illustrates our boundary to hone in on “red giants,” sources that are brighter and redder than points on that line yet still within our selection zone. This choice helps identify candidates that are close to the cluster of known symbiotic stars around M_G of -2 and bp_rp of 2 .

the HR diagram. In contrast, only 10% of our candidates lie in this red giant zone. For candidates with a 95% probability of being a symbiotic star ($P \geq 0.95$), this fraction rises to 30% — these sources are indicated in Figure 7 with dark green symbols. While the ML classifier does not require sources to lie in the zone defined by Equation (4), it evidently recognizes the importance of cool giants to the identification of symbiotic stars.

We selected sources not just on position in the HR diagram but on a requirement that their Gaia spectrum match our template (Fig. 4). Figure 8 illustrates, showing the mean low-resolution spectrum of stars in our catalog, including individual spectra of the highest probability sources ($P \geq 95\%$). The basic spectral features include significant H_α emission and possible molecular absorption, with some variability in the strength of these

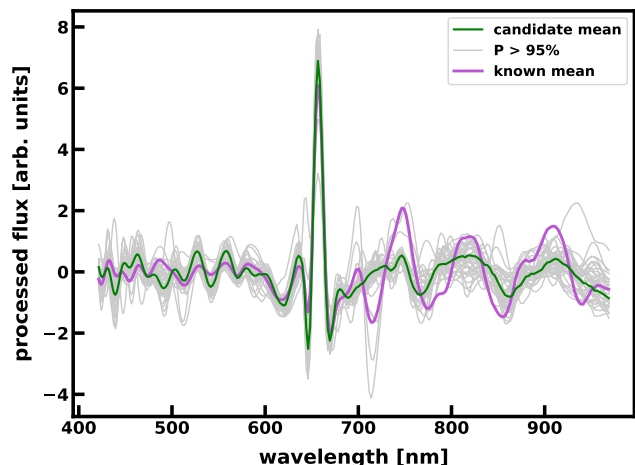


FIG. 8.— GDR BP+RP spectra of symbiotic star candidates. The thick purple curve is the mean spectrum of known symbiotic stars, the green curve is the average spectrum of all candidate stars, while the thin curves are individual spectra.

features, as seen with the individual spectra of our top candidates.

As an independent check on our candidates’ properties, we show available optical, NIR, and WISE color indices of our candidates in Figure 9, similar to (cf. Fig. 2). The overlap in the color-color plane with known symbiotic stars is strong. The candidates lie in a more restricted range of G-J and J-K values, and are on average slightly ($\lesssim 0.5$ mag) bluer than the known symbiotic stars, similar to the distribution in the HR diagram (Fig. 7). Our candidates’ WISE colors also overlap with those of known symbiotic stars. There is a strong clustering in both populations around 0.5-1 mag in W1-W3, and 1-2 mag in W2-W4, with our candidates on average slightly redder than the known symbiotic star population. We interpret these clusters in optical, NIR, and WISE colors as emission from an unobscured giant, as in S-type symbiotic stars.

Figure 9 shows color-color outliers among our candidates. These sources are up to several magnitudes redder than the bulk of the stars considered here. Our interpretation, as with the known symbiotic stars, is that these

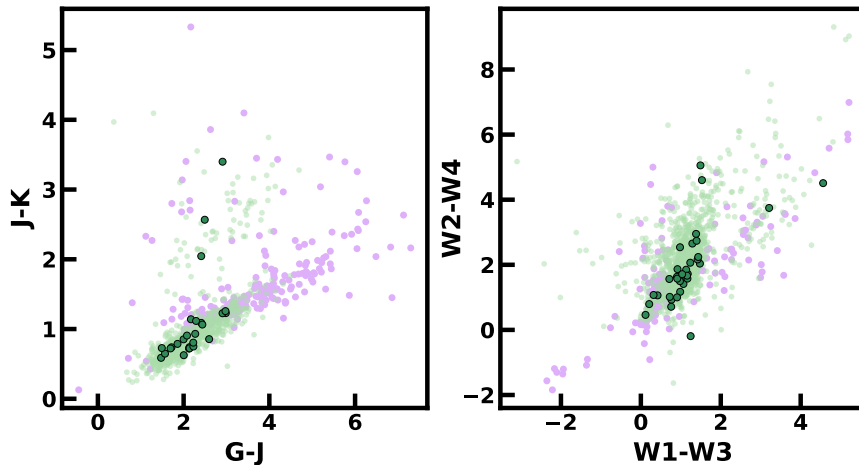


FIG. 9.— Optical, near infrared and WISE colors for symbiotic star candidates, similar to Figure 2. The candidates are distributed in roughly the same way in these color-color diagrams as known symbiotic stars.

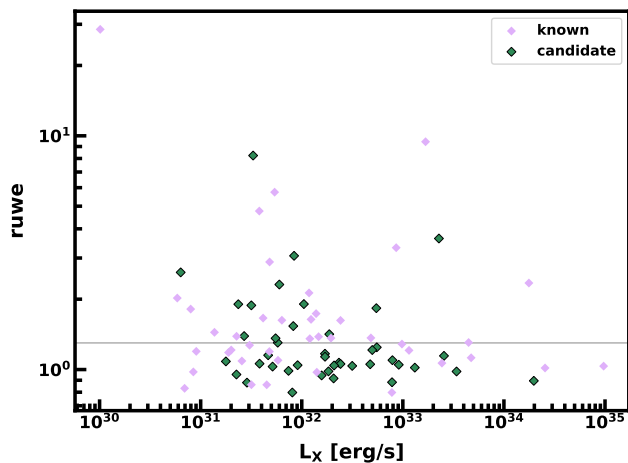


FIG. 10.— Gaia’s astrometric measure $ruwe$ versus X-ray luminosity of candidate symbiotic stars. Candidates introduced in this work are in green, while the light purple symbols indicate known symbiotic stars.

outliers are in a dusty environment, like D-type symbiotic stars.

We emphasize that our candidate selection is entirely determined with Gaia data, and that optical-NIR-WISE colors offer an independent avenue for comparisons between candidates and known symbiotic stars.

Finally, to acknowledge the potential importance of X-ray emission and binarity to the identification of symbiotic stars, in Figure 10 we plot X-ray luminosity and astrometric uncertainty ($ruwe$). As in §3, we draw X-ray fluxes from *ROSAT*, *SRG/eROSITA*, and *XMM-Newton* wide-field observations, adopting the geometric distances of Bailer-Jones et al. (2021) to derive X-ray luminosity, L_X . The spread of $ruwe$ values is broad (compare with Fig. 3), with a third of our X-ray emitting candidates showing $ruwe$ greater than 1.3, a marker of binarity with separations of a few astronomical units, as expected for symbiotic stars.

4.1. Sources with high promise

With the properties of symbiotic stars explored as in §3, these findings highlight the effectiveness of our classifier in isolating potential symbiotic systems from the GDR3 dataset and mark a significant step toward expanding the known catalog of symbiotic stars. Further spectroscopic follow-up is necessary to confirm their symbiotic nature and refine the classification model.

We can nonetheless make progress in honing in on sources with high promise as symbiotic star candidates. We begin by selecting candidates from our catalog of 1,674 stars that have an 80% probability or better of being a symbiotic star. Of these, we consider only those with X-ray emission associated with them. The result is a group of 25 high-promise stars, listed in Table 3. The table includes $ruwe$ and L_X , both of which can bolster the case for interpreting these sources as symbiotic stars along with other spectral and photometric attributes.

Table 3 also includes a column indicating whether a source is associated with a red giant. Our motivation for including this indicator stems from Figures 1 and 7. They illustrate that symbiotic stars, while distributed over a range of colors and magnitudes, tend to cluster in the region of the HR diagram associated with red giants (Eq. (4)). This yields nine stars noted in the table by “o” in the Red Giant column.

We further highlight a subset of manually selected candidates from our broader sample of 1,674 stars that were not included in Tables 2 and 3 but demonstrate intriguing characteristics suggestive of symbiotic behavior. These selections are based on a combination of high $ruwe$ values, strong projection coefficients (S values), and favorable SIMBAD object types (o-types), particularly those identified as emission-line stars (EM*), X-ray sources (X), or long-period variables (LP*). While their ML probabilities may not place them among the highest-ranked candidates, these additional observational features warrant further notation. One such candidate is Gaia DR3 524428838421397760, which exhibits a very high $ruwe$ value of 9.990 and a strong projection coefficient (S value) of 1.24. SIMBAD identifies this source as EM GGA 2*, a long-period variable star. Although it lacks associated X-ray information, being one of the highest $ruwe$ values in our sample makes it a compelling

TABLE 3
CANDIDATES WITH ASSOCIATED X-RAY EMISSION

Gaia DR3 Source_ID	RA (degrees)	Dec (degrees)	BP-RP	M_G	Ruwe	S	p	L_X (erg/s)	Red Giant
5862963206161616640	191.9614122	-62.9959058	1.113	-2.863	1.903	1.11	0.97	2.36×10^{31}	o
4067633238255477248	268.3685113	-24.7743574	1.088	-2.883	3.636	1.28	0.96	2.27×10^{33}	o
4155000844481174656	278.3656995	-10.5901248	1.988	1.879	8.233	1.17	0.96	3.30×10^{31}	
511373821468521600	26.8679812	61.8075708	1.852	-0.038	1.906	1.18	0.94	1.05×10^{32}	
5350304330466080768	161.4879820	-59.9453074	1.590	-0.723	3.066	1.32	0.94	8.39×10^{31}	
5333423903245046912	123.6864290	-41.7564811	1.493	-0.285	1.360	1.01	0.93	5.51×10^{31}	
3429108971530640000	88.1401270	25.7640650	1.346	-1.664	2.311	1.24	0.93	6.00×10^{31}	
4146612395388085376	274.6617474	-13.7789734	1.436	-0.506	1.831	1.32	0.93	5.47×10^{32}	
4256506967717461120	280.2504364	-5.4643725	2.447	-3.016	1.391	1.23	0.92	2.69×10^{31}	o
5337634962895857792	167.7367796	-60.7061083	1.488	-1.401	1.245	1.09	0.91	5.53×10^{32}	
4097811804449201664	275.3833836	-16.2233348	1.559	0.860	1.535	1.24	0.90	8.24×10^{31}	
2060601411718713088	304.8842007	37.2875676	1.177	-1.270	2.604	1.13	0.89	6.34×10^{30}	
5866068158280977536	210.2027359	-62.2514152	2.314	0.420	1.169	1.08	0.89	1.70×10^{32}	
4323101294616761472	293.4896372	18.4139288	2.105	-0.897	1.303	1.11	0.88	5.78×10^{31}	o
5963997295254312064	253.3623541	-45.4071775	1.669	-0.268	1.041	1.23	0.85	2.09×10^{32}	
4319930096909297664	290.3915616	14.8824531	2.161	-4.331	0.982	1.28	0.85	1.84×10^{32}	o
276644757710014976	64.9255612	55.9993607	1.584	-2.622	1.144	1.28	0.85	2.55×10^{33}	o
5255677056923564544	156.0766151	-57.8082591	2.730	-1.456	1.048	1.01	0.84	9.12×10^{32}	o
5866510642950541952	213.5103447	-61.6919817	1.327	-1.417	1.070	1.25	0.84	2.33×10^{32}	
2067537096694188416	305.5259549	40.4465447	2.528	1.232	1.083	1.23	0.83	1.78×10^{31}	
3441214006141133952	84.6512611	26.5049398	1.348	0.039	1.152	1.03	0.82	4.65×10^{31}	
5976051206857091200	261.1779942	-34.1958969	2.441	2.905	1.057	1.02	0.82	2.42×10^{32}	
5966221298030125056	254.7781823	-42.7023476	2.173	-0.531	1.882	1.26	0.81	3.17×10^{31}	o
519352324516039680	23.9577173	66.2120235	2.003	-1.427	1.054	1.29	0.81	4.75×10^{32}	o
4153412355116242688	277.1774747	-11.2828971	2.469	1.747	1.096	1.02	0.81	7.89×10^{32}	

NOTE. — Column L_X is the total X-ray flux in erg/s. The column listed as Red Giant, denoted by a lower case (o), is stars found by Eq 4 indicated above the grey line in our selection zone in Figure 7.

symbiotic candidate.

Gaia DR3 5888269634519939712 presents a similarly strong case with $S = 1.43$, one of the highest in our sample, and a *ruwe* value of 1.090, lower than that of EM* GGA 2 but still noteworthy. This star is listed in SIMBAD as [M81] I-468, also categorized as a long-period variable. Like the previous star, it shows no X-ray emission, yet its projection coefficient places it among the more promising candidates.

Lastly, Gaia DR3 6725263992006252160 also has an unusually high S value of 1.43. It is identified in SIMBAD as EM* AS 276, a long-period variable candidate. Despite the absence of X-ray data, this object-type designation indicating variability, along with the photometric and spectral features highlighted here, strengthens this source’s potential as a symbiotic star.

5. CONCLUSION

Symbiotic stars offer important windows into stellar and binary evolution. When composed of a red giant and a main sequence companion, a symbiotic star evolves into a cataclysmic variable. With a white dwarf companion, the next evolutionary step is a white dwarf binary. Both channels give rise to Type Ia supernovae (Munari & Renzini 1992b; Di Stefano 2010), standard candles that are essential in astrophysical cosmology (Brout et al. 2022).

Stellar evolution theory and stellar population synthesis tie together our understanding of symbiotic stars and their prevalence in the Milky Way (Kenyon 1986; Munari & Renzini 1992a; Magrini et al. 2003; Lü et al. 2006; Akras 2023; Xu et al. 2024). Yet predictions exceed reality by a factor of ten or more. One reason is the cool giant dominates the light at optical wavebands, so symbiotic stars hide among other giant stars in photometric

surveys. Another reason is that these stars are variable in their spectral features (e.g., Merc & Boffin 2025). Recent surveys (e.g. Akras et al. 2019a,b, 2021; Akras 2023; Jia et al. 2023; Chen et al. 2025) have made progress, but a gap still remains between detections and theoretical predictions.

Our project stems from a desire to improve this situation. We worked with the Gaia Data Release 3 archive, identifying a subset of 171 known symbiotic stars observed with Gaia’s low resolution spectrometers. We defined selection criteria in color, magnitude, astrometric quality, and a projection coefficient (S in Eq. (3)) that measures how well-matched a Gaia spectrum is to the characteristic spectrum of a symbiotic star. Noting that other factors may help to identify these stars, including astrometric uncertainties because of binarity, we trained a machine-learning classifier to provide a refined list of candidates from the 1.8 billion Gaia sources.

The result is a catalog of 1,674 symbiotic star candidates. We recommend follow-up observations for all of these sources. In some cases where we have X-ray counterparts, we are most confident that we have identified new symbiotic stars, and recommend prioritizing these sources for further study.

Our approach balances accuracy in astrometry, brightness of candidates, and broad spectral features to search for new symbiotic candidates. While our study has limitations, including the brightness cuts and dependence on a single spectral template, future work could improve upon this to cast a wider and more effective net. The rewards would be significant. With each new discovery comes the potential for a deeper understanding of stellar evolution and the stars that have revolutionized our understanding of the universe.

ACKNOWLEDGMENTS

SEB is grateful for support from the Undergraduate Research Opportunity Program at the University of Utah. This research has made use of the SIMBAD

database (Wenger et al. 2000), and the VizieR catalog access tool (Ochsenbein et al. 2000), operated at CDS, Strasbourg, France. We are thankful for the availability of these resources.

REFERENCES

- Akras, S. 2023, *MNRAS*, 519, 6044, doi: 10.1093/mnras/stad096
- Akras, S., Gonçalves, D. R., Alvarez-Candal, A., & Pereira, C. B. 2021, *MNRAS*, 502, 2513, doi: 10.1093/mnras/stab195
- Akras, S., Guzman-Ramirez, L., Leal-Ferreira, M. L., & Ramos-Larios, G. 2019a, *ApJS*, 240, 21, doi: 10.3847/1538-4365/aaf88c
- Akras, S., Leal-Ferreira, M. L., Guzman-Ramirez, L., & Ramos-Larios, G. 2019b, *MNRAS*, 483, 5077, doi: 10.1093/mnras/sty3359
- Allen, D. A. 1984, *PASA*, 5, 369, doi: 10.1017/S132335800017215
- Aschenbach, B., Bräuninger, H., Briel, U., et al. 1981, *Space Sci. Rev.*, 30, 569, doi: 10.1007/BF01246075
- Bailer-Jones, C. A. L., Rybizki, J., Fouesneau, M., Demleitner, M., & Andrae, R. 2021, *AJ*, 161, 147, doi: 10.3847/1538-3881/abd806
- Bath, G. T. 1977, *MNRAS*, 178, 203, doi: 10.1093/mnras/178.2.203
- Belczyński, K., Mikolajewska, J., Munari, U., Ivison, R. J., & Friedjung, M. 2000, *A&AS*, 146, 407, doi: 10.1051/aas:2000280
- Blind, N., Boffin, H. M. J., Berger, J. P., et al. 2011, *A&A*, 536, A55, doi: 10.1051/0004-6361/201118036
- Bonnarel, F., Fernique, P., Bienaymé, O., et al. 2000, *A&AS*, 143, 33, doi: 10.1051/aas:2000331
- Boyarchuk, A. A. 1969, *Communications of the Konkoly Observatory Hungary*, 65, 395
- Brou, D., Scolnic, D., Popovic, B., et al. 2022, *ApJ*, 938, 110, doi: 10.3847/1538-4357/ac8e04
- Bujarrabal, V., Alcolea, J., Mikolajewska, J., Castro-Carrizo, A., & Ramstedt, S. 2020, *A&A*, 633, C1, doi: 10.1051/0004-6361/201833633e
- Buss, Jr., R. H., & Snow, Jr., T. P. 1988, *ApJ*, 335, 331, doi: 10.1086/166931
- Castro-Ginard, A., Penoyre, Z., Casey, A. R., et al. 2024, *A&A*, 688, A1, doi: 10.1051/0004-6361/202450172
- Chen, J., Wang, L., Li, Y.-B., et al. 2025, arXiv e-prints, arXiv:2506.09352, doi: 10.48550/arXiv.2506.09352
- Cutri, R. M., Wright, E. L., Conrow, T., et al. 2013, *Explanatory Supplement to the AllWISE Data Release Products*, Explanatory Supplement to the AllWISE Data Release Products, by R. M. Cutri et al.
- Di Stefano, R. 2010, *ApJ*, 719, 474, doi: 10.1088/0004-637X/719/1/474
- Freund, S., Czesla, S., Predehl, P., et al. 2024, *A&A*, 684, A121, doi: 10.1051/0004-6361/202348278
- Gaia Collaboration, Vallenari, A., Brown, A. G. A., et al. 2023, *A&A*, 674, A1, doi: 10.1051/0004-6361/202243940
- Green, G. M., Schlafly, E., Zucker, C., Speagle, J. S., & Finkbeiner, D. 2019, *ApJ*, 887, 93, doi: 10.3847/1538-4357/ab5362
- Hachisu, I., Kato, M., & Nomoto, K. 1999, *ApJ*, 522, 487, doi: 10.1086/307608
- Healy, S., Horiuchi, S., Colomer Molla, M., et al. 2024, *Monthly Notices of the Royal Astronomical Society*, 529, 3630, doi: 10.1093/mnras/stae738
- Hunsch, M., Schmitt, J. H. M. M., & Voges, W. 1998, *A&AS*, 127, 251, doi: 10.1051/aas:1998347
- Jansen, F., Lumb, D., Altieri, B., et al. 2001, *A&A*, 365, L1, doi: 10.1051/0004-6361:20000036
- Jia, Y., Guo, S., Zhu, C., et al. 2023, *Research in Astronomy and Astrophysics*, 23, 105012, doi: 10.1088/1674-4527/ace9b2
- Kenyon, S. J. 1986, *The symbiotic stars* (Cambridge University Press)
- Kenyon, S. J., & Fernandez-Castro, T. 1987, *AJ*, 93, 938, doi: 10.1086/114379
- Kenyon, S. J., Livio, M., Mikolajewska, J., & Tout, C. A. 1993, *ApJ*, 407, L81, doi: 10.1086/186811
- Kenyon, S. J., & Webbink, R. F. 1984, *ApJ*, 279, 252, doi: 10.1086/161888
- Kervella, P., Arenou, F., & Thévenin, F. 2022, *A&A*, 657, A7, doi: 10.1051/0004-6361/202142146
- Liu, Z.-W., Röpké, F. K., & Han, Z. 2023, *Research in Astronomy and Astrophysics*, 23, 082001, doi: 10.1088/1674-4527/acd89e
- Lü, G., Yungelson, L., & Han, Z. 2006, *MNRAS*, 372, 1389, doi: 10.1111/j.1365-2966.2006.10947.x
- Luna, G. J. M., Sokoloski, J. L., Mukai, K., & Nelson, T. 2013, *A&A*, 559, A6, doi: 10.1051/0004-6361/201220792
- Magrini, L., Corradi, R. L. M., & Munari, U. 2003, in *Astronomical Society of the Pacific Conference Series*, Vol. 303, *Symbiotic Stars Probing Stellar Evolution*, ed. R. L. M. Corradi, J. Mikolajewska, & T. J. Mahoney, 539, doi: 10.48550/arXiv.astro-ph/0208085
- Merc, J., & Boffin, H. M. J. 2025, *A&A*, 695, A61, doi: 10.1051/0004-6361/202553789
- Merc, J., Gális, R., & Wolf, M. 2019, *Research Notes of the American Astronomical Society*, 3, 28, doi: 10.3847/2515-5172/ab0429
- Merc, J., Mikolajewska, J., Gromadzki, M., et al. 2020, *A&A*, 644, A49, doi: 10.1051/0004-6361/202039132
- Merrill, P. W., & Humason, M. L. 1932, *PASP*, 44, 56, doi: 10.1086/124191
- Munari, U. 2019, arXiv e-prints, arXiv:1909.01389, doi: 10.48550/arXiv.1909.01389
- Munari, U., & Renzini, A. 1992a, *ApJ*, 397, L87, doi: 10.1086/186551
- . 1992b, *ApJ*, 397, L87, doi: 10.1086/186551
- Munari, U., Traven, G., Masetti, N., et al. 2021, *MNRAS*, 505, 6121, doi: 10.1093/mnras/stab1620
- Ochsenbein, F., Bauer, P., & Marcout, J. 2000, *A&AS*, 143, 23, doi: 10.1051/aas:2000169
- Payne-Gaposchkin, C. 1946, *ApJ*, 104, 362, doi: 10.1086/144866
- Pearce, L. A., Males, J. R., Weinberger, A. J., et al. 2022, *MNRAS*, 515, 4487, doi: 10.1093/mnras/stac2056
- Planquart, L., Jorissen, A., & Van Winckel, H. 2025, *A&A*, 694, A85, doi: 10.1051/0004-6361/202452833
- Predehl, P., Hasinger, G., Böhringer, H., et al. 2006, in *Society of Photo-Optical Instrumentation Engineers (SPIE) Conference Series*, Vol. 6266, *Space Telescopes and Instrumentation II: Ultraviolet to Gamma Ray*, ed. M. J. L. Turner & G. Hasinger, 62660P, doi: 10.1117/12.670249
- Riess, A. G., Filippenko, A. V., Challis, P., et al. 1998, *AJ*, 116, 1009, doi: 10.1086/300499
- Schmitt, J. H. M. M., Hünsch, M., Schneider, P. C., et al. 2024, *A&A*, 688, A9, doi: 10.1051/0004-6361/202449181
- Shapley, H. 1923, *Harvard College Observatory Bulletin*, 783, 3
- Stassun, K. G., & Torres, G. 2021, *ApJ*, 907, L33, doi: 10.3847/2041-8213/abdaad
- Swings, P., & Struve, O. 1941, *ApJ*, 93, 356, doi: 10.1086/144272
- Webb, N. A., Coriat, M., Traulsen, I., et al. 2020, *A&A*, 641, A136, doi: 10.1051/0004-6361/201937353
- Webbink, R. F., Livio, M., Truran, J. W., & Orio, M. 1987, *ApJ*, 314, 653, doi: 10.1086/165095
- Webster, B. L., & Allen, D. A. 1975, *MNRAS*, 171, 171, doi: 10.1093/mnras/171.1.171
- Wenger, M., Ochsenbein, F., Egret, D., et al. 2000, *A&AS*, 143, 9, doi: 10.1051/aas:2000332
- White, N. E., Giommi, P., & Angelini, L. 2000, *VizieR Online Data Catalog: The WGACAT version of ROSAT sources* (White+ 2000), *VizieR On-line Data Catalog: IX/31*. Originally published in: *Laboratory for High Energy Astrophysics (LHEA/NASA), Greenbelt* (2000)
- Whiting, M. L., Hill, J. B., Bromley, B. C., & Kenyon, S. J. 2023, *AJ*, 165, 193, doi: 10.3847/1538-3881/acc526
- Wright, E. L., Eisenhardt, P. R. M., Mainzer, A. K., et al. 2010, *AJ*, 140, 1868, doi: 10.1088/0004-6256/140/6/1868

Xu, X.-j., Shao, Y., & Li, X.-D. 2024, ApJ, 962, 126,
doi: [10.3847/1538-4357/ad20ec](https://doi.org/10.3847/1538-4357/ad20ec)

Zucker, C., Saydjari, A. K., Speagle, J. S., et al. 2025, arXiv
e-prints, arXiv:2503.02657, doi: [10.48550/arXiv.2503.02657](https://doi.org/10.48550/arXiv.2503.02657)

This paper was built using the Open Journal of Astrophysics L^AT_EX template. The OJA is a journal which

provides fast and easy peer review for new papers in the **astro-ph** section of the arXiv, making the reviewing process simpler for authors and referees alike. Learn more at <http://astro.theoj.org>.